



# The solubility of N<sub>2</sub> in silicate melts and nitrogen partitioning between upper mantle minerals and basalt

Hans Keppler<sup>1</sup> · Laura Cialdella<sup>1</sup> · Frédéric Couffignal<sup>2</sup> · Michael Wiedenbeck<sup>2</sup>

Received: 7 March 2022 / Accepted: 4 July 2022 / Published online: 13 August 2022  
© The Author(s) 2022

## Abstract

The solubility of N<sub>2</sub> in basaltic (MORB) and haplogranitic melts was studied at oxidizing conditions (oxygen fugacity about two log units above the Ni–NiO buffer). Under these conditions, N<sub>2</sub> is expected to be the only significant nitrogen species present in the melt. Experiments were carried out from 0.1 to 2 GPa and 1000–1450 °C using either an externally heated TZM pressure vessel, an internally heated gas pressure vessel or a piston cylinder apparatus. Nitrogen contents in run product glasses were quantified by SIMS (secondary ion mass spectrometry). To discriminate against atmospheric contamination, <sup>15</sup>N-enriched AgN<sub>3</sub> was used as the nitrogen source in the experiments. According to infrared and Raman spectra, run product glasses contain N<sub>2</sub> as their only dissolved nitrogen species. Due to interactions with the matrix, the N<sub>2</sub> molecule becomes slightly infrared active. Nitrogen solubility in the melts increases linearly with pressure over the entire range studied; the effect of temperature on solubility is small. The data may, therefore, be described by simple Henry constants  $K_{\text{haplogranite}} = (1461 \pm 26)$  ppm N<sub>2</sub>/GPa and  $K_{\text{MORB}} = (449 \pm 21)$  ppm N<sub>2</sub>/GPa, recalculated to ppm by weight (μg/g) of isotopically normal samples. These equations describe the solubility of nitrogen during MORB generation and during melting in the crust, as we show by thermodynamic analysis that N<sub>2</sub> is the only significant nitrogen species in these environments. Nitrogen solubility in the haplogranitic melt is about three times larger than for the MORB melt, as is expected from ionic porosity considerations. If expressed on a molar basis, nitrogen solubility is significantly lower than argon solubility, in accordance with the larger size of the N<sub>2</sub> molecule. Notably, N<sub>2</sub> solubility in felsic melts is also much lower than CO<sub>2</sub> solubility, even on a molar basis. This implies that the exsolution of nitrogen may drive vapor oversaturation in felsic melts derived from nitrogen-rich sediments. We also measured the partitioning of nitrogen between olivine, pyroxenes, plagioclase, garnet, and basaltic melt by slowly cooling MORB melts to sub-liquidus temperatures to grow large crystals. The mineral/melt partition coefficients of nitrogen range from 0.001 to 0.002, and are similar to argon partition coefficients. These new data, therefore, support the assumption that there is little fractionation between nitrogen and argon during mantle melting and that the N<sub>2</sub>/Ar ratio in basalts and xenoliths is, therefore, representative of the N<sub>2</sub>/Ar ratio in the mantle source. This assumption is essential for assessing the size of the nitrogen reservoir in the mantle. Our data also show that for an upper mantle oxidation state that is similar to the one observed today, nitrogen outgassing by partial melting is extremely efficient and even low melt fractions in the range of a few percent may extract nearly all nitrogen from the mantle source.

**Keywords** Nitrogen · Solubility · Partitioning · Silicate melt · Argon · N<sub>2</sub>/argon ratio · Mantle reservoir · Degassing

## Introduction

Among the volatile elements on Earth (H, C, N, S, noble gases), the geochemical behavior of nitrogen is probably the least well understood. N<sub>2</sub> is the main constituent of the atmosphere, and nitrogen occurs in all living organisms as an essential component of amino acids, proteins, nucleobases, RNA, and DNA. The near-surface nitrogen cycle between organic matter, oceans, and the atmosphere has been extensively studied (e.g., Karl et al., 1997). In the form

---

Communicated by Othmar Müntener.

---

✉ Hans Keppler  
hans.keppler@uni-bayreuth.de

<sup>1</sup> Bayerisches Geoinstitut, Universität Bayreuth, 95440 Bayreuth, Germany

<sup>2</sup> Deutsches GeoForschungsZentrum GFZ, 14473 Potsdam, Germany

of ammonium ( $\text{NH}_4^+$ ) ions derived from decaying organic matter, nitrogen may also enter sediments, where  $\text{NH}_4^+$  mostly substitutes for  $\text{K}^+$  in sheet silicates (e.g., Busigny et al. 2003). However, the magnitude of the nitrogen reservoirs in the Earth's interior is difficult to infer, and the uncertainty of such estimates generally increases with depth (e.g., Marty 1995; Johnson and Goldblatt 2015). Moreover, the cycling of nitrogen between Earth's interior and the surface is not easy to study; one obvious problem is the difficulty to discriminate nitrogen in volcanic gases from contamination by air (e.g., Sano et al. 2001; Labidi et al. 2020).

The isotopic composition of nitrogen in the atmosphere is very different from that of most comets (Marty and Yokochi 2006). It is, therefore, likely that nitrogen, the main component of the atmosphere was not delivered by some cometary bodies during the latest stages of accretion, but instead originated from the degassing of Earth's interior, probably after solidification of a magma ocean. On the modern Earth, the deep cycle of nitrogen is driven by nitrogen recycling in subduction zones (e.g., Busigny et al. 2003) and outgassing at midocean ridges, ocean islands, and continental hotspot volcanoes (e.g., Sano et al. 2001). All of these processes depend on the solubility of nitrogen in silicate melts and on the partitioning of nitrogen between silicate melts and mantle minerals. Previous studies have shown that the behavior of nitrogen in magmatic systems depends very strongly on oxygen fugacity. Over a wide range of oxygen fugacities,  $\text{N}_2$  is the main nitrogen species dissolved in silicate melts and in fluids, while only at rather reducing conditions, species of  $\text{N}^{3-}$  become more significant (e.g., Libourel et al. 2003; Roskosz et al. 2006; Mysen et al. 2008; Kadik et al. 2011; Li and Keppler 2014; Boulliong et al. 2020; Bernadou et al. 2021). Under anhydrous conditions, this switch in nitrogen oxidation state requires oxygen fugacities below the Fe–FeO buffer (e.g., Libourel et al. 2003). In the presence of water, however, noticeable fractions of reduced species, in particular  $\text{NH}_3$  and  $\text{NH}_4^+$  may already be observed at more oxidizing conditions. A comprehensive study of nitrogen solubility in melts and of nitrogen partitioning between silicate melts and minerals would therefore have to consider the effects of temperature, pressure, and oxygen fugacity. However, the oxygen fugacity in the modern-day upper mantle is far above the Fe–FeO buffer (Frost and McCammon 2008) with most of Earth's crust being even more oxidized. Under these conditions,  $\text{N}_2$  is expected to be the only significant nitrogen species in silicate melts and aqueous fluids. We, therefore, carried out a systematic study of  $\text{N}_2$  solubility in basaltic (MORB) and felsic (haplogranitic) melts, as well as some exploratory experiments on nitrogen partitioning between mantle minerals and basaltic melt under conditions where  $\text{N}_2$  should predominate in the melt phase. We will use these data primarily to compare the behavior of  $\text{N}_2$  with Ar and to experimentally test whether fractionation between  $\text{N}_2$  and

Ar may occur during mantle melting. Since the correlation of  $\text{N}_2$  with Ar is an essential tool for estimating the mantle inventory of nitrogen (Marty 1995; Johnson and Goldblatt 2015), any possible fractionation between these two species would have severe consequences for our understanding of Earth's deep nitrogen budget.

## Experimental methods

### Starting materials

Synthetic glasses were used as starting materials for the solubility experiments. A MORB glass with a composition similar to an average midocean ridge basalt (Gale et al. 2013) was prepared by mixing stoichiometric amounts of analytical grade  $\text{SiO}_2$ ,  $\text{TiO}_2$ ,  $\text{Al}(\text{OH})_3$ ,  $\text{Fe}_2\text{O}_3$ ,  $\text{Mg}(\text{OH})_2$ ,  $\text{CaCO}_3$ ,  $\text{Na}_2\text{CO}_3$ , and  $\text{K}_2\text{CO}_3$  and grinding the mixture for 1 h under ethanol. After drying, the powder was transferred into a Pt crucible and heated over 12 h with a constant rate to 1100 °C, after which the temperature was kept constant for another 12 h. The sample was then melted in air at 1600 °C in a high-temperature furnace and quenched in distilled water. The resulting black glass was crushed and used as starting material in  $\text{N}_2$  solubility experiments with MORB composition. A haplogranitic glass with a composition equivalent to 40 wt.% albite, 35 wt.% quartz and 25 wt.% orthoclase was prepared by a similar procedure. The glass was colorless with abundant gas bubbles and was crushed before use. The compositions of the starting glasses are compiled in Table 1. In some partitioning experiments, the MORB glass was mixed with 15–30 wt.% of a mixture of MgO and  $\text{SiO}_2$  in  $\text{Mg}_2\text{SiO}_4$  (“olivine”) or  $\text{MgSiO}_3$  (“orthopyroxene”) composition to saturate crystalline phases. Silver azide  $\text{AgN}_3$  enriched with > 98% in the  $^{15}\text{N}$  isotope was prepared from  $^{15}\text{N}$ -enriched  $\text{NaN}_3$  (Eurisotop) and  $\text{AgNO}_3$  following the procedure described by Keppler (1989). Upon heating to 300 °C, silver azide decomposes to  $\text{N}_2$  and Ag. In the interpretation of our data, we will assume that there is a negligible difference between the solubility and partitioning behavior of  $^{15}\text{N}$  and isotopically normal nitrogen (mostly  $^{14}\text{N}$ ).

### High-pressure experiments

Solubility and partitioning experiments were carried out at 0.1–0.5 GPa in an internally heated gas pressure vessel (IHPV) with rapid-quench device and from 1 to 3 GPa in an end-loaded piston cylinder apparatus. For the IHPV experiments, 1–5 mg of  $\text{Ag}^{15}\text{N}_3$  was sealed (arc welded) together with 50–100 mg of glass powder into Pt capsules (20 mm long, 3.5 mm outer diameter, 0.15 mm wall thickness). A Harwood IHPV vessel rated to a maximum pressure of 1 GPa was used in vertical orientation. The pressure medium

**Table 1** Composition of starting glasses (in wt.%)

|                                | HPG      | MORB     |
|--------------------------------|----------|----------|
| SiO <sub>2</sub>               | 77.0 (1) | 49.7 (7) |
| TiO <sub>2</sub>               | –        | 1.72 (4) |
| Al <sub>2</sub> O <sub>3</sub> | 13.3 (7) | 14.1 (1) |
| MgO                            | –        | 8.1 (1)  |
| CaO                            | –        | 10.8 (1) |
| FeO <sub>tot</sub>             | –        | 10.1 (1) |
| Na <sub>2</sub> O              | 4.4 (3)  | 2.93 (7) |
| K <sub>2</sub> O               | 4.2 (1)  | 0.18 (1) |
| Total                          | 98.9     | 97.6     |

Compositions were measured by electron microprobe. Numbers in parentheses are one standard deviation in the last digits. Data are averages of about 20 individual analyses. Note that total iron oxide is given as FeO<sub>tot</sub>; since the glass was melted in air, it may mostly contain Fe<sub>2</sub>O<sub>3</sub>, which would increase the total of MORB by about 1 wt.%

HPG haplogranite, MORB midocean ridge basalt

was argon, though as the samples were sealed in Pt capsules, the argon had no access to them. The sample capsules were suspended on a Pt wire, which could be fused by a voltage pulse for quenching, causing the sample to drop into the cold zone of the autoclave at the end of an experiment. Temperature was measured by two type S thermocouples located near the upper and lower ends of the capsule. A two-zone heater with Mo wires was adjusted such that during the experiment, no temperature gradient was measurable along the sample. Pressure was measured with a manganin cell with an uncertainty of less than 1%. A few experiments at 0.1 GPa and temperatures up to 1100 °C were also carried out in externally heated pressure vessels made of the TZM alloy (Ti and Zr enforced Mo), again using argon as pressure medium. In these experiments, the capsule was mounted at the end of a filler rod with a magnetic piece at the bottom. For quenching, an outer magnet holding the filler rod was removed such that the sample dropped into a water-cooled zone and was quenched to nearly room temperature within 1–2 s.

For piston cylinder experiments, usually 4–7 mg of AgN<sub>3</sub> and about 150 mg of glass powder (or of a glass oxide mix, see above) were sealed into cylindrical Pt<sub>95</sub>Rh<sub>5</sub> capsules with lids at the end (10 mm long, 5 mm outer diameter, 0.3 mm wall thickness). A ½ inch talc pyrex assembly with a tapered graphite heater was used for the experiments. Temperatures were measured with a type S thermocouple nearly touching the sample. A friction correction of 18% was applied to the nominal pressure on the piston, as derived from the

hydraulic oil pressure. Solubility runs were carried out at constant temperature, while partitioning experiments were first heated to some temperature above the liquidus for a few hours to completely melt the charge, then very slowly cooled down a constant ramp rate to the final run temperature between the liquidus and the solidus of the system and then kept at this temperature for several days. All experiments were quenched by shutting of the heating current, which caused the sample to cool almost to room temperature within about 30 s.

## Analytical methods

Sample capsules were weighed and checked for leaks before and after the experiments. After the runs, capsules were opened and the contents embedded in epoxy blocks and polished. Phases were identified and analyzed by a JEOL JXA-8200 electron microprobe. These measurements were carried out with 15 kV acceleration voltage, 15 nA beam current, 20 s counting time on peak, and 10 s on background. Calibrants used were andradite for Si and Ca, MnTiO<sub>3</sub> for Ti, spinel for Al, Fe metal for Fe, enstatite for Mg, albite for Na and orthoclase for K.

SIMS measurements of <sup>15</sup>N were carried out with the Cameca 1280-HR ion probe at GFZ Potsdam, using a protocol similar to that described by Yoshioka et al. (2018). Polished sample capsules embedded in epoxy were coated with a 35 nm thick high-purity gold layer. Individual analyses used a <sup>16</sup>O<sup>-</sup> primary ion beam focused to a ~15 μm diameter spot with a total impact energy of 23 keV and 20–24 nA primary beam current. The mass resolution was set at ~2500 (10% of peak height) and data were collected in mono-collection depth profiling mode. Each measurement cycle included <sup>28</sup>Si<sup>2+</sup>, <sup>14</sup>N<sup>+</sup> and <sup>15</sup>N<sup>+</sup>. Our SIMS calibration was based on <sup>15</sup>N-implanted synthetic MORB and rhyolite glasses. Nitrogen-free glass samples were implanted with <sup>15</sup>N at the Institute of Ion Beam Physics and Materials Research at the Helmholtz Zentrum Dresden-Rossendorf, with three different peak concentrations equivalent to 100, 300, and 10,000 μmol/mol. Synthetic buddingtonite with natural isotopic composition was also measured under the same condition as the calibration materials to establish the analytical mass fractionation of our SIMS method. Nearly all of our analyses of experimental products yielded <sup>15</sup>N<sup>+</sup>/<sup>14</sup>N<sup>+</sup> ≥ 1, such that the background was less than 1% of total nitrogen in all but the most depleted of cases. The best-fit linear regressions for the MORB and rhyolite implant series yielded relative sensitivity factors that agreed within 1.5%. Based on all our observations, we believe our data are reliable at better than a 10% uncertainty. For the analyses of olivine, pyroxenes, and garnet, the ion-implanted mineral standards described by Li et al. (2013) were used. Nitrogen

in plagioclase was quantified using the glass standards described above.

## Spectroscopic methods

Raman spectra of glasses and fluid inclusions were measured in backscatter geometry using a Horiba LabRam 800 HR UV confocal Raman spectrometer. The 514 nm line of an argon laser at 200 mW output power was used for excitation. Spectra were recorded using a 50× objective with a 1800 mm<sup>-1</sup> grating and a Peltier-cooled CCD detector. The spectroscopic resolution was about 5 cm<sup>-1</sup>. Accumulation times of 2 × 120 s per spectral segment were typically used. For measuring glass spectra, the cut, but not yet polished surfaces of the samples were used, to minimize interferences from defects caused by mechanical damage to the glass. Fluid inclusions were measured through polished surfaces. To reduce interferences from atmospheric N<sub>2</sub>, a spectrum of air measured under the same conditions as the sample was always subtracted from the sample spectrum.

Infrared spectra were measured on doubly polished glass slabs with a Bruker IFS 120 HR Fourier-transform infrared spectrometer coupled to a microscope with all-reflecting, Cassegrainian optics (Bruker IRscope I). A tungsten light source, CaF<sub>2</sub> beam splitter, and a narrow-band MCT detector

were used for the measurements. For each sample, up to 2000 scans were accumulated at 4 cm<sup>-1</sup> resolution. Water and CO<sub>2</sub> contents were quantified using the extinction coefficients given by Shishkina et al. (2010).

Mössbauer spectra were collected at room temperature on flat slices of glass approximately 300 μm thick (7 mg Fe/cm<sup>2</sup>). A 1.5 mm diameter hole in a piece of Pb foil was placed over the central part of each sample. Spectra were recorded in transmission mode on a constant acceleration Mössbauer spectrometer with a nominal 370 MBq <sup>57</sup>Co high specific activity source in a 12 μm thick Rh matrix. The velocity scale was calibrated relative to Fe foil. Each spectrum was collected for two days.

## Results and discussion

### Solubility experiments

Table 2 gives a summary of the N<sub>2</sub> solubility experiments. Run products were glasses either completely free of crystals or they contained only traces of crystalline phases. Gas bubbles, indicating vapor saturation were often observed. The haplogranitic glasses were colorless or slightly greenish or bluish in hue due to colloidal

**Table 2** Summary of experiments on nitrogen solubility in silicate melts

| Run no | Starting material | Glass (mg) | Ag <sup>15</sup> N <sub>3</sub> (mg) | Apparatus | P (GPa) | T (°C) | Duration (hours) | Nitrogen (μg/g <sup>15</sup> N) |
|--------|-------------------|------------|--------------------------------------|-----------|---------|--------|------------------|---------------------------------|
| a1     | HPG               | 64         | 1.6                                  | TZM       | 0.1     | 1000   | 24               | 120 (1)                         |
| a2     | HPG               | 50         | 2.1                                  | TZM       | 0.1     | 1100   | 24               | 130 (1)                         |
| a5     | HPG               | 88         | 4.5                                  | IHPV      | 0.3     | 1100   | 4                | 507 (1)                         |
| a3     | HPG               | 73         | 2.0                                  | IHPV      | 0.3     | 1200   | 6                | 455 (6)                         |
| a4     | HPG               | 75         | 2.0                                  | IHPV      | 0.3     | 1300   | 4                | 397 (4)                         |
| a9     | HPG               | 93         | 4.0                                  | IHPV      | 0.4     | 1300   | 6                | 117 (1)                         |
| a10    | HPG               | 91         | 3.9                                  | IHPV      | 0.4     | 1400   | 4                | 602 (18)                        |
| b1     | HPG               | 141        | 1.7                                  | PC        | 1       | 1200   | 6                | 1576 (339)                      |
| b2     | HPG               | 153        | 2.7                                  | PC        | 1       | 1300   | 6                | 1923 (75)                       |
| b5     | HPG               | 141        | 7.0                                  | PC        | 2       | 1300   | 6                | 3002 (529)                      |
| b6     | HPG               | 135        | 4.9                                  | PC        | 2       | 1300   | 6                | 3222 (69)                       |
| c17    | MORB              | 122        | 4.2                                  | IHPV      | 0.1     | 1400   | 4                | 46 (7)                          |
| c8     | MORB              | 109        | 3.6                                  | IHPV      | 0.3     | 1300   | 4                | 165 (1)                         |
| c9     | MORB              | 93         | 3.3                                  | IHPV      | 0.3     | 1400   | 4                | 139 (59)                        |
| c7     | MORB              | 108        | 4.4                                  | IHPV      | 0.45    | 1400   | 3                | 88 (13)                         |
| d1     | MORB              | 142        | 4.3                                  | PC        | 1       | 1300   | 6                | 541 (271)                       |
| d2     | MORB              | 144        | 4.3                                  | PC        | 1       | 1400   | 6                | 573 (7)                         |
| d3     | MORB              | 147        | 6.6                                  | PC        | 1.5     | 1400   | 6                | 701 (10)                        |
| d4     | MORB              | 136        | 5.8                                  | PC        | 2       | 1450   | 6                | 929 (55)                        |

Numbers in parentheses are one standard deviation in the last digits. Glass and Ag<sup>15</sup>N<sub>3</sub> are the amounts of HPG or MORB glass and of Ag<sup>15</sup>N<sub>3</sub> initially loaded into the capsule

HPG haplogranite, MORB midocean ridge basalt, TZM rapid-quench TZM cold seal pressure vessel, IHPV internally heated gas pressure vessel, PC piston cylinder apparatus, P pressure, T temperature

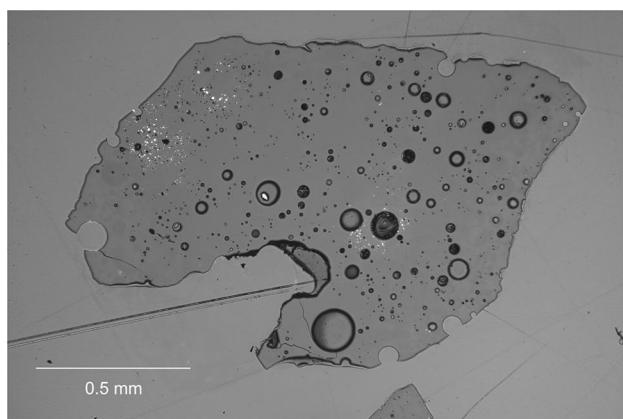


**Fig. 1** Run product glass from experiment a2 on  $N_2$  solubility in haplogranitic melt as seen in reflected light. Abundant gas bubbles are seen in the clear glass, indicating vapor saturation. Bright particles are silver grains from the decomposition of  $AgN_3$

silver and they almost always contained abundant bubbles (Fig. 1). The MORB glasses were nearly black and only occasionally included a few bubbles. This is likely due to the much lower viscosity of the MORB melt, which allowed any gas bubble to rapidly segregate out. In any case, the amount of  $N_2$  initially loaded into the capsules was always larger than that detected in the samples, such that vapor saturation should have been achieved. With few exceptions (see below), our synthetic glasses appeared homogeneous without obvious signs of nitrogen zonation in the SIMS measurements. Indeed, according to published diffusion coefficients of N in silicate melts (Frischat et al. 1978) the run durations should be more than sufficient to reach equilibrium, in particular as the starting material was a fine-grained ( $< 50 \mu m$ ) glass powder, meaning that the required diffusion distance to reach equilibrium was short. The volatile-free silicate bulk composition of the glasses measured after the solubility experiments was essentially identical to the starting composition. Even FeO contents were within 5% (relative) of the original FeO content of the MORB glass, indicating negligible iron loss, as expected from the short run durations and the oxidized state of the starting glass prepared in air.

For constraining the redox conditions during the runs, Mossbauer spectra of MORB glasses from piston cylinder and internally heated gas pressure vessel experiments are shown in Fig. 2. The data show a high ( $Fe^{3+}/Fe^{2+}$ ) ratio, attesting to highly oxidizing conditions. Using the calibration of Borisov et al. (2018), the redox state of iron was converted into oxygen fugacity. For sample d4 from a piston cylinder experiment at 2 GPa, 1450 °C, with a  $Fe^{3+}/Fe^{2+}$  ratio of 0.92 (Fig. 2a), this yielded an oxygen fugacity of 2.4 log units above the Ni–NiO buffer. Sample c8 from an experiment in the internally heated gas pressure vessel at 0.3

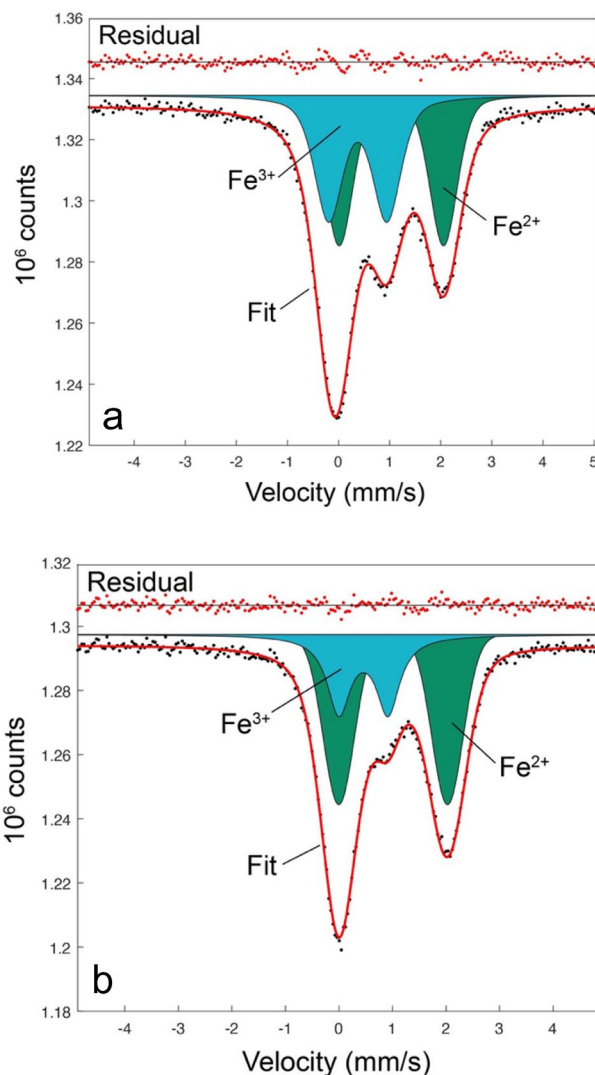


**Fig. 2** Mossbauer spectra of run product MORB glasses. **a** Sample d4 from a piston cylinder experiment at 2 GPa, 1450 °C, yielding a  $Fe^{3+}/Fe^{2+}$  ratio of 0.92. **b** Sample c8 from an experiment in the internally heated gas pressure vessel at 0.3 GPa and 1300 °C, yielding a  $Fe^{3+}/Fe^{2+}$  ratio of 0.52

GPa and 1300 °C, with a  $Fe^{3+}/Fe^{2+}$  ratio of 0.52 (Fig. 2b), indicated a log  $fO_2$  of Ni–NiO + 1.8.

Figure 3 shows  $N_2$  solubility in haplogranitic and MORB melt as a function of pressure. To a good approximation, the  $N_2$  concentration in the melt was found to be proportional to pressure over the entire range studied. Nitrogen solubility may therefore be described by a simple Henry constant  $K$ , with  $K_{\text{haplogranite}} = (1552 \pm 52) \text{ ppm } ^{15}N_2/\text{GPa}$  ( $R^2 = 0.994$ ) and  $K_{\text{MORB}} = (481 \pm 22) \text{ ppm } ^{15}N_2/\text{GPa}$  ( $R^2 = 0.991$ ). The Henry constants were obtained by a linear fit of the data constrained to pass through the origin. The two apparently anomalous experiments a9 (haplogranite) and c7 (MORB) were excluded. These two samples

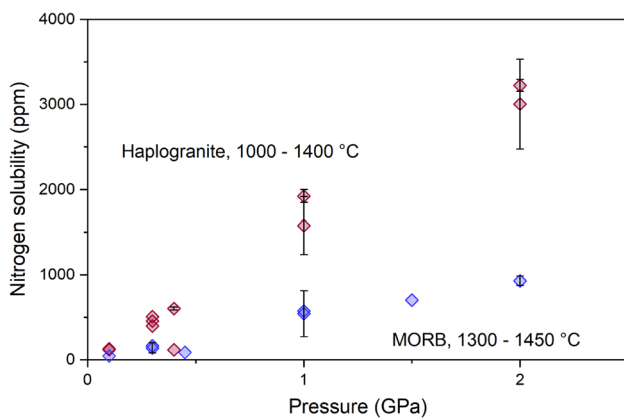


**Fig. 3**  $^{15}\text{N}_2$  solubility in haplogranite melt and MORB melt as a function of pressure. Error bars are one standard deviation. Where no error bars are shown, the uncertainty is smaller than the size of the symbol

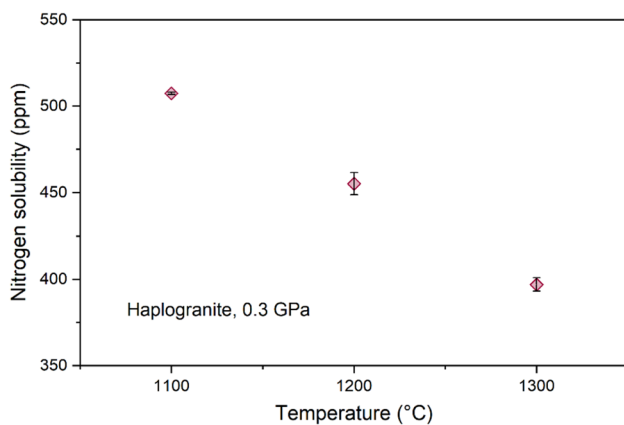


**Fig. 4** Temperature dependence of  $^{15}\text{N}_2$  solubility in haplogranitic melt at 0.3 GPa. Error bars are one standard deviation

may not have been vapor-saturated, possibly due to minor leakage during the experiment. Recalculated to ppm (by weight;  $\mu\text{g/g}$ ) of isotopically normal nitrogen, the Henry constants are  $K_{\text{haplogranite}} = (1449 \pm 49)$  ppm  $\text{N}_2/\text{GPa}$  and  $K_{\text{MORB}} = (449 \pm 21)$  ppm  $\text{N}_2/\text{GPa}$ .

Compared to the effect of pressure on solubility, the effect of temperature is subordinate. As shown in Fig. 4,  $\text{N}_2$  solubility in haplogranitic melt at 0.3 GPa appears to systematically decrease with temperature. However, at higher pressures of 1 GPa and above, the data in Table 2 rather suggest a reversal of this trend. A similar effect is known from studies of the solubility of water in silicate melts, where the solubility decreases with temperature at low pressures, while it increases at higher pressures above 0.5 GPa (Holtz et al. 1995). This behavior can be understood from entropy considerations. Increasing temperature should always favor the state with higher entropy. At low pressures, the silicate melt

coexists with a low-density fluid of high entropy and therefore, increasing temperature should favor the partitioning of nitrogen into the fluid. However, at higher pressures, the fluid phase becomes more liquid like, such that the entropy difference between the two phases decreases. In this situation, the mixing entropy in both phases contributes strongly to the overall entropy. Mixing entropy alone would favor an equal distribution of nitrogen between the two phases, with the effect that increasing temperature then increases  $\text{N}_2$  solubility in the silicate melt.

### Comparison with previous studies of nitrogen solubility in silicate melts

The results presented here are the first data on the solubility of a pure  $\text{N}_2$  fluid in a felsic or basaltic melt up to 2 GPa. Most previous studies were carried out under rather reducing conditions, where several species of nitrogen may coexist and/or in systems where the fluid phase coexisting with the melt contained other volatile species, such as water as well (Mallik et al. 2018; Bernadou et al. 2021). Libourel et al. (2003) and Miyazaki et al. (2004) reported Henry coefficients for the dissolution of  $\text{N}_2$  in basaltic melts derived from experiments at 1 bar. Miyazaki et al. give a range of  $(3\text{--}5) \cdot 10^{-9}$  mol  $\text{N}_2 \text{ g}^{-1} \text{ atm}^{-1}$ , while Libourel et al. (2003) reports a value of  $(2.21 \pm 0.53) \cdot 10^{-9}$  mol  $\text{N}_2 \text{ g}^{-1} \text{ atm}^{-1}$  at 1425 °C. The latter value would correspond to  $(6188 \pm 1484)$  ppm/GPa. Obviously, this number is about one order of magnitude higher than the Henry coefficient derived here from our experiments at higher pressure. However, considering that these data are based on experiments that range over more than four orders of magnitude in pressure, the similarity of the Henry constants is remarkable. The difference between the low-pressure values and those observed here could be due to the fact that the compressibility of silicate melts markedly decreases with pressure (Bottinga 1985; Wang et al. 2014). This means that in the range of very low pressures, a significant compaction of the melt occurs, which may reduce the pore space available to accommodate molecules such as  $\text{N}_2$ . However, in particular for experiments carried out at 1 bar under oxidizing conditions, nitrogen solubility in the melt is so low that quantification may be difficult; the associated uncertainties may also contribute to the differences between the experimental data sets.

Mallik et al. (2018) measured nitrogen contents in silicic melts in equilibrium with a nitrogen-rich fluid phase at 2–4 GPa, 1050–1300 °C and oxygen fugacities ranging from close to the Ni–NiO buffer to 4 log units below this buffer. They observed nitrogen contents ranging from 0.4 to 1 wt.%, which are not very different from the data reported here in the haplogranitic system, considering the differences in pressure. The somewhat higher solubilities observed by Mallik et al. (2018) may perhaps be due to minor amounts

of dissolved  $\text{NH}_3$  in the melt, in addition to the predominant  $\text{N}_2$ . Curiously, an early study by Kesson and Holloway (1974) reports a Henry constant of about 2000 ppm/GPa for albitic melts, derived from experiments with a mixed  $\text{N}_2$  containing fluid phase at 0.44 GPa. This value is very close to that reported here for haplogranitic composition. However, Kesson and Holloway (1974) do not provide any details on the analytical methods used for measuring nitrogen, making a detailed comparison difficult. Finally, Carroll and Webster (1994) predicted a solubility of  $\text{N}_2$  in silicate melts in the order of 750–1500 ppm/GPa, depending on composition, and assuming that  $\text{N}_2$  behaves similarly to Ar. This prediction is remarkably close to the experimental data obtained here.

Bernadou et al (2021) proposed a general model of nitrogen solubility in basaltic melts as a function of pressure, temperature, and oxygen fugacity, valid to 1 GPa. In this model, bulk solubility is given as the sum of  $\text{N}_2$  solubility and of  $\text{N}^{3-}$  solubility, the latter only being relevant at reduced conditions.  $\text{N}_2$  solubility is described as  $c(\text{N}_2) = k_b f\text{N}_2$ , where  $f\text{N}_2$  is  $\text{N}_2$  fugacity and  $k_b$  is a thermodynamic equilibrium constant, depending on pressure and temperature. For 0.1 GPa, this equation describes the  $\text{N}_2$  solubility measured in MORB at 1400 °C reasonably well. However, with increasing pressure, the Bernadou et al. (2021) model more and more underestimates nitrogen solubility, up to about an order of magnitude at 1 GPa. The reason for this is likely a rather high value for  $\Delta V$ , the volume change of the melt upon dissolution of  $\text{N}_2$ . This value is given as 4 J/bar mol, which corresponds to 40  $\text{cm}^3/\text{mol}$ . However, the molar volume of liquid nitrogen at ambient pressure is only 34.7  $\text{cm}^3/\text{mol}$  and it appears implausible that the partial molar volume in the melt at high pressure should be larger—it should rather be considerably smaller. The Bernadou et al. (2021) model is a regression fit of nitrogen solubility data covering a wide range of redox conditions. The discrepancy with our measurements illustrates that for deriving any reliable solubility model, measurements of nitrogen solubility under conditions where  $\text{N}_2$  is definitively the only species present are essential.

### Nitrogen speciation in quenched glasses and fluid inclusions

Figure 5 shows Raman spectra of a fluid inclusion inside glass and of quenched haplogranitic glass alone from our high-pressure solubility experiments. Only bands due to  $\text{N}_2$  can be seen, no other nitrogen species were detected. In particular, no bands due to ammonium or other N–H species are observed in the 3000–3300  $\text{cm}^{-1}$  range. Due to the doping with  $^{15}\text{N}$ , the stretching frequency of  $^{15}\text{N}_2$  is shifted relative to  $^{14}\text{N}_2$  which is the predominant isotope species of natural nitrogen, i.e., in air, by a factor of  $(14/15)^{1/2} = 0.966$ . This

frequency shift allows a reliable distinction of nitrogen in the sample from atmospheric  $\text{N}_2$ . From the ratio of the  $^{14}\text{N}^{15}\text{N}$  band to the  $^{15}\text{N}_2$  band, the isotopic purity of the  $\text{N}_2$  in the sample can be estimated to be 98–99%, in agreement with the specification of the isotopically enriched  $\text{NaN}_3$  used to produce  $\text{AgN}_3$  and further confirmed during our SIMS analyses. The spectra of quenched MORB glasses look similar to the haplogranitic glass shown in Fig. 5a, but the intensities of the  $\text{N}_2$  bands are much weaker due to the lower nitrogen solubility in such melts.

A FTIR spectrum of a haplogranitic glass saturated with  $\text{N}_2$  at 2 GPa is shown in Fig. 6. As  $\text{N}_2$  is not infrared active, it should not be detectable in infrared spectra. However, there is a band at 2253  $\text{cm}^{-1}$ , essentially identical in position with the  $^{15}\text{N}_2$  band seen in the Raman spectra of both glasses and fluid inclusions. Very likely, the  $^{15}\text{N}_2$  molecules dissolved in the glass matrix became infrared active by the interaction with the glass matrix, which induced dipoles. A similar effect is known for  $\text{H}_2$  molecules dissolved in a glass matrix (Schmidt et al. 1998). From the infrared spectrum shown in Fig. 6 and the nitrogen content of this sample of 3222 ppm  $^{15}\text{N}$  (Table 2), the infrared extinction coefficients of  $^{15}\text{N}_2$  in haplogranitic glass can be estimated, assuming a density of 2300 g/liter. This yields a linear extinction coefficient of 6.37  $\text{L mol}^{-1} \text{cm}^{-1}$  and an integral extinction coefficient of 83.2  $\text{L mol}^{-1} \text{cm}^{-2}$ .

No evidence for any other nitrogen species, in particular of reduced nitrogen, e.g.,  $\text{NH}_3$  or  $\text{NH}_4^+$ , is detectable either in the Raman or in the infrared spectra. No evidence for the nitrosyl species suggested by Roskosz et al. (2006) was found either. In a series of nitrogen-containing glasses synthesized in the piston cylinder apparatus, Roskosz et al. (2006) had detected a Raman band near 2100  $\text{cm}^{-1}$ , which they assigned to NO. We note, however, that a Raman band at a very similar position may also be caused by carbon monoxide (CO) in the quenched glass (Yoshioka et al. 2015). Carbon contamination may occur in piston cylinder runs at high temperature (Brooker et al. 1998) and the glasses studied by Roskosz et al. (2006) were prepared from carbonate as starting material, such that the presence of CO cannot be confidently excluded.

Our spectroscopic data confirm that  $\text{N}_2$  was the only nitrogen species present in the fluid phase and the only significant nitrogen species dissolved in the silicate melts. This is consistent with the high oxygen fugacity prevailing during the experiments and with the fact that the decomposition of  $\text{AgN}_3$  upon heating only produces  $\text{N}_2$  (Keppler 1989). Moreover,  $\text{N}_2$  is kinetically inert and extremely unreactive, such that even under conditions where it should be reduced to other nitrogen species, very long-run durations and sometimes the presence of a catalyst, such as Pt powder, are required to convert it into different nitrogen species (Li and Keppler 2014). While oxygen fugacity was not

**Fig. 5** Raman spectra of **a** quenched haplogranitic glass (experiment b5) and **b** of a fluid inclusion (experiment a10). Note the absence of bands due to ammonium or other N–H species in the 3000–3300  $\text{cm}^{-1}$  frequency range of the glass spectrum (**a**). The ratio of the  $^{14}\text{N}^{15}\text{N}$  band to the  $^{15}\text{N}_2$  band can be used to estimate the isotopic purity of  $\text{N}_2$  in the sample. This ratio is 0.034 for spectrum **a** and 0.021 for spectrum **b**. The  $^{14}\text{N}_2$  band is probably mostly due to air in front of the sample

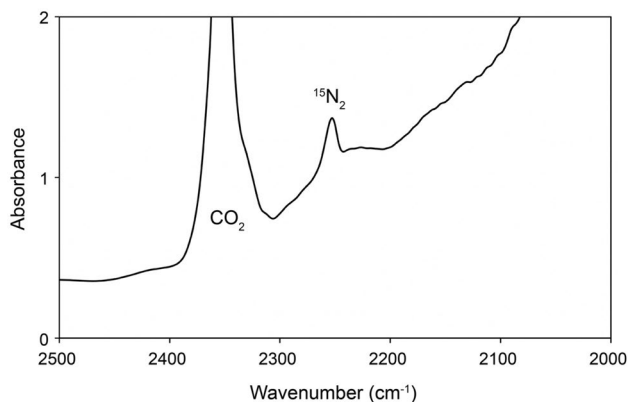
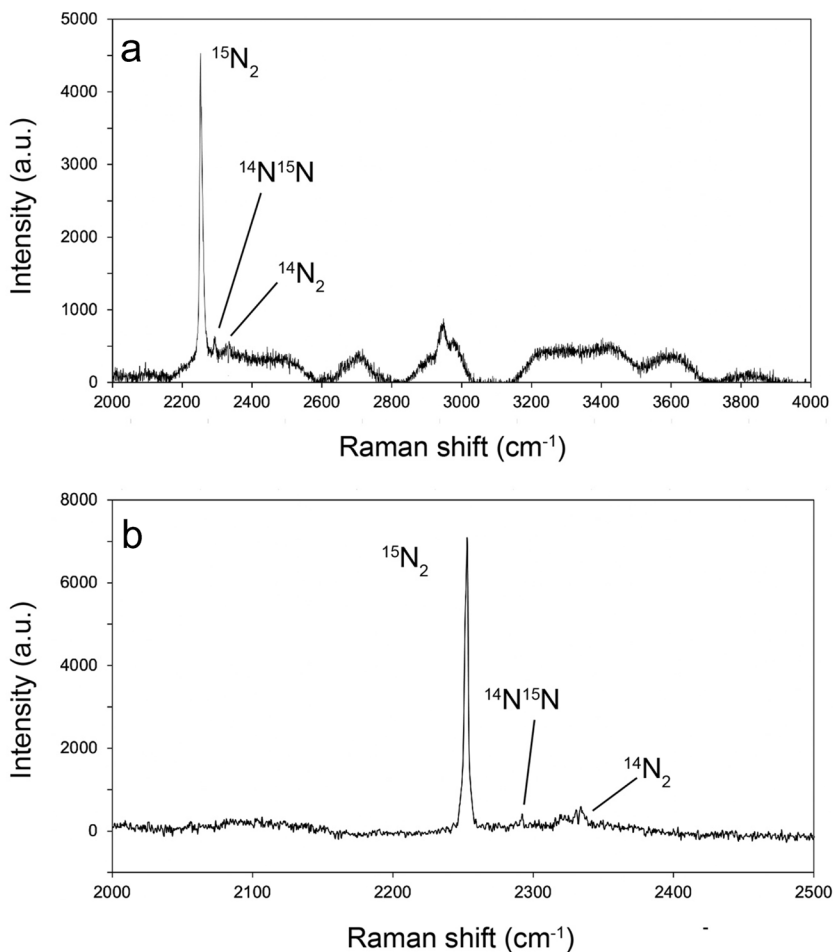


**Fig. 6** Detail of the infrared spectrum of a quenched haplogranitic glass (run b6). This is an uncorrected raw spectrum from a 1.755 mm thick sample. A band of  $^{15}\text{N}_2$  dissolved in the glass is detectable. While  $\text{N}_2$  should not be infrared active, the interaction with the glass matrix may induce dipoles, which make the molecule infrared active. The band of molecular  $\text{CO}_2$  in the glass is due to a minor carbon contamination, probably from the carbonates used to make the starting glasses

strictly buffered in our experiments, the Mössbauer spectra of quenched MORB glasses (Fig. 2) show that it was about two log units above the Ni–NiO buffer.

The glasses from piston cylinder experiments typically contained <0.5 wt.% of  $\text{H}_2\text{O}$  and <0.1 wt.% of  $\text{CO}_2$ . Since water will partition strongly into the silicate melt, this means that the fluid coexisting with the melt is basically dry and very pure  $\text{N}_2$ . According to the water solubility law of Shishkina et al. (2010), 0.5 wt.% of  $\text{H}_2\text{O}$  in a basaltic melt corresponds to a water partial pressure of only 3.7 MPa, which is negligible to the total pressure of the experiments. Concentrations in samples from IHPV experiments were even lower. The traces of  $\text{CO}_2$  may still be inherited from the carbonate starting materials used for glass synthesis at 1 bar.

### A comparison of $\text{N}_2$ and Ar solubilities

Figure 7 compares the nitrogen solubilities obtained in the current study with the argon solubilities in granitic and basaltic melt as measured by White et al. (1989), Carroll and Stolper (1993), Schmidt and Keppeler (2002), and Iacono-Marziano et al. (2010). In both types of silicate melts,  $\text{N}_2$

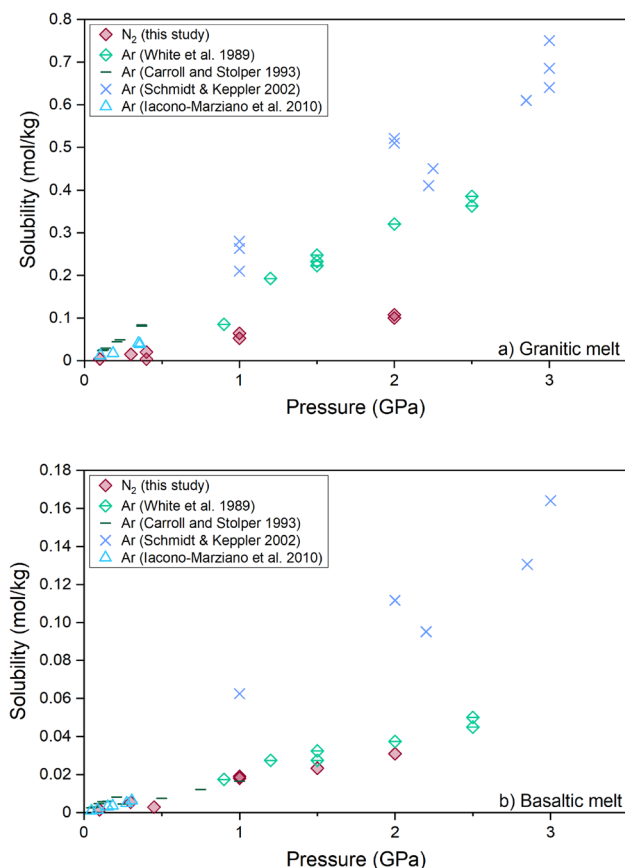


**Fig. 7** Comparison of N<sub>2</sub> solubility and Ar solubility in granitic melt (a) and basaltic melt (b). N<sub>2</sub> solubility data (red circles) are from the current study. Ar solubility data are from White et al. (1989), Carroll and Stolper (1993), Schmidt & Keppler (2002), and Iacono-Marziano et al. (2010). The Ar solubility data by Schmidt & Keppler refer to a Fe-free melt with higher silica content than for the other results shown here

is less soluble than Ar, with the difference being particularly large for the granitic melt. The lower solubility of N<sub>2</sub> would be consistent with the larger size of the N<sub>2</sub> molecule as compared to the Ar atom. From studies of noble gases, it is known that the solubility of noble gases in silicate melts generally decreases with the size of the noble gas atom, possibly because the population of suitable “cavities” in the silicate melt decreases with size (e.g., Carroll and Webster 1994 and references therein). It is not straightforward, however, to compare the size of a spherical atom like Ar with that of a non-spherical molecule such as N<sub>2</sub>. One possibility here is to compare the molar volumes of the liquids at their boiling points at 1 bar. For liquid nitrogen, the density is 0.807 g cm<sup>-3</sup> at -196 °C, while for Ar it is 1.398 g cm<sup>-3</sup> at -185 °C. This translates into a molar volume of Ar in the liquid state of 28.57 cm<sup>3</sup> mol<sup>-1</sup>, as compared to 34.72 cm<sup>3</sup> mol<sup>-1</sup> for N<sub>2</sub>. This comparison confirms that indeed the N<sub>2</sub> molecule will require more space than the Ar atom under

similar conditions; in addition, the non-spherical geometry of the N<sub>2</sub> may have some influence on the overall solubility.

The increase of N<sub>2</sub> solubility from basaltic to haplogranitic melt is rather similar to that observed for noble gases, particularly argon (Fig. 7). This suggests that the compositional dependence of N<sub>2</sub> solubility may be related to ionic porosity as is often assumed for noble gases (e.g., Carroll and Webster 1994 and references therein). Ionic porosity generally decreases with the NBO/T (non-bridging oxygen atoms per tetrahedron) parameter, but for N<sub>2</sub>, the relationship of solubility with ionic porosity may be more easily visualized than that with the NBO/T parameter.

## Partitioning experiments

By slow cooling of MORB melts—some of which were doped with an excess of Mg<sub>2</sub>SiO<sub>4</sub> or MgSiO<sub>3</sub> component or with natural almandine powder—from super-liquidus temperatures, it was possible to grow large, sometimes mm-sized crystals of olivine, pyroxenes, garnet, and plagioclase (Figs. 8, 9). Nitrogen partition coefficients derived from SIMS analyses of such crystals and coexisting residual melts are compiled in Table 3. Bulk chemical analyses of the phases in these experiments are given in Table 4. Because of the much longer run duration and because of the addition of hygroscopic MgO to the starting material in some partitioning experiments, the glass samples have elevated H<sub>2</sub>O contents up to 3.2 wt.%, as compared to the nearly “dry” solubility experiments. The long-run durations also caused significant iron loss (Table 4), but due to the poly-phase nature of these products, the extent of bulk iron loss is hard to quantify.

Mineral/melt partition coefficients of N<sub>2</sub> range from about 0.001–0.002, indicating a generally highly incompatible behavior of nitrogen. A similar range of partition coefficients was already estimated by Li et al. (2013) for Ni–NiO buffer conditions at 2 GPa and 1300 °C. The single value of  $D^{\text{px/melt}} = 0.00013$  from run 3.18 appears to be anomalously low. This is likely related to the fact that in this experiment, the nitrogen concentration in the melt was particularly high (0.4 wt.%) and the low partition coefficient may reflect some saturation effect in the crystal lattice. All other partition coefficients are similar, without any obvious dependence on crystal structures or compositions. The fact that even for Al-rich pyroxenes (see Table 4), the partition coefficients are not higher than for olivine, essentially rules out any contribution of ammonium ions (NH<sub>4</sub><sup>+</sup>) to nitrogen solubility in the minerals, since this type of substitution mechanism would be very much favored by coupled substitutions such as the replacement of Ca<sup>2+</sup> + Mg<sup>2+</sup> by NH<sub>4</sub><sup>+</sup> and Al<sup>3+</sup> (Li et al. 2013). Very likely, N<sub>2</sub> is incorporated in vacancies or Schottky defects in these minerals.

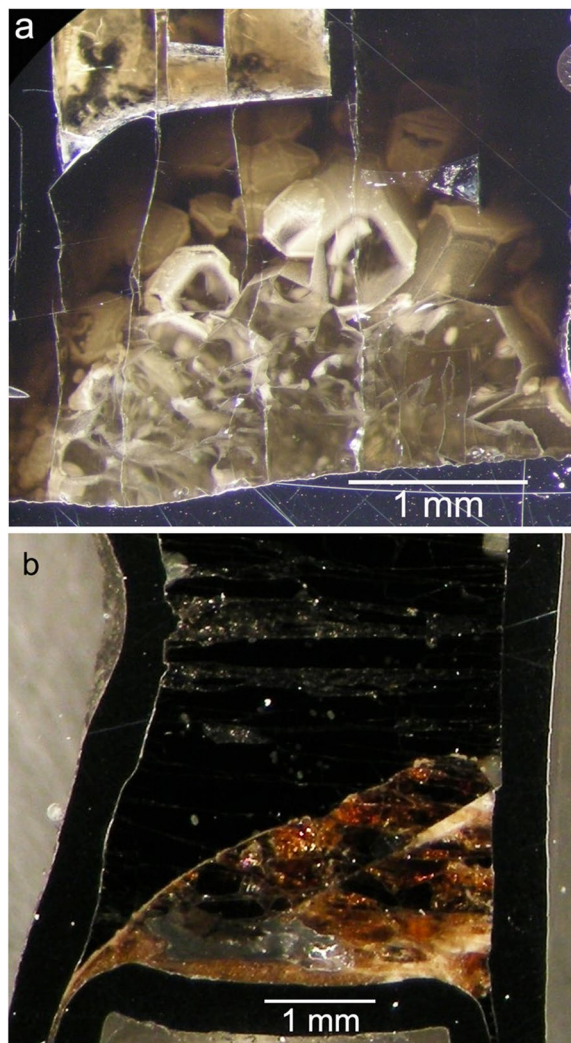


**Fig. 8** Optical images of run products from partitioning experiments. **a** Large crystals of orthopyroxene crystallized from a MORB melt at 1.5 GPa and 1400–1300 °C (Run 8.24). **b** Crystals of red garnet at the bottom of a capsule together with residual MORB melt, quenched to a black glass (Run 21.45, 4 GPa, 1620–1500 °C)

Figure 10 compares the partition coefficients of nitrogen with those for argon by Heber et al. (2007). The two datasets overlap, but the nitrogen partition coefficients tend to be higher, though it must be noted that the uncertainties in both data sets are considerable.

### Relevance of N<sub>2</sub> solubility and partitioning data for mantle melting and degassing

Since our experiments were carried out under rather oxidizing conditions and N<sub>2</sub> was the only nitrogen species detected in the run product glasses, the possible applicability of these data to melting and degassing processes, in particular in the upper mantle, requires some discussion. In natural, water-bearing melts and fluids, N<sub>2</sub> and NH<sub>3</sub> appear to be the

major nitrogen species (e.g., Li and Keppler 2014). They are related to each other through the equilibrium



with the equilibrium constant  $K_N$

$$K_N = \frac{f_{\text{NH}_3}^2}{f_{\text{N}_2} f_{\text{H}_2}^3}, \quad (2)$$

where  $f$  are the fugacities of the relevant species.

Hydrogen (H<sub>2</sub>) fugacity is related to water fugacity and oxygen fugacity through the reaction



with the equilibrium constant

$$K_w = \frac{f_{\text{H}_2} f_{\text{O}_2}^{1/2}}{f_{\text{H}_2\text{O}}}. \quad (4)$$

Equations (2) and (4) may be combined to yield

$$\frac{f_{\text{NH}_3}^2}{f_{\text{N}_2}} = K_N K_w^3 \frac{f_{\text{H}_2\text{O}}^3}{f_{\text{O}_2}^{3/2}}. \quad (5)$$

As one may see from Eq. (5), the equilibrium between reduced (NH<sub>3</sub>) and oxidized (N<sub>2</sub>) nitrogen species does not only depend on oxygen fugacity, but also on water fugacity—and the effect of water fugacity is actually much stronger than that of oxygen fugacity.

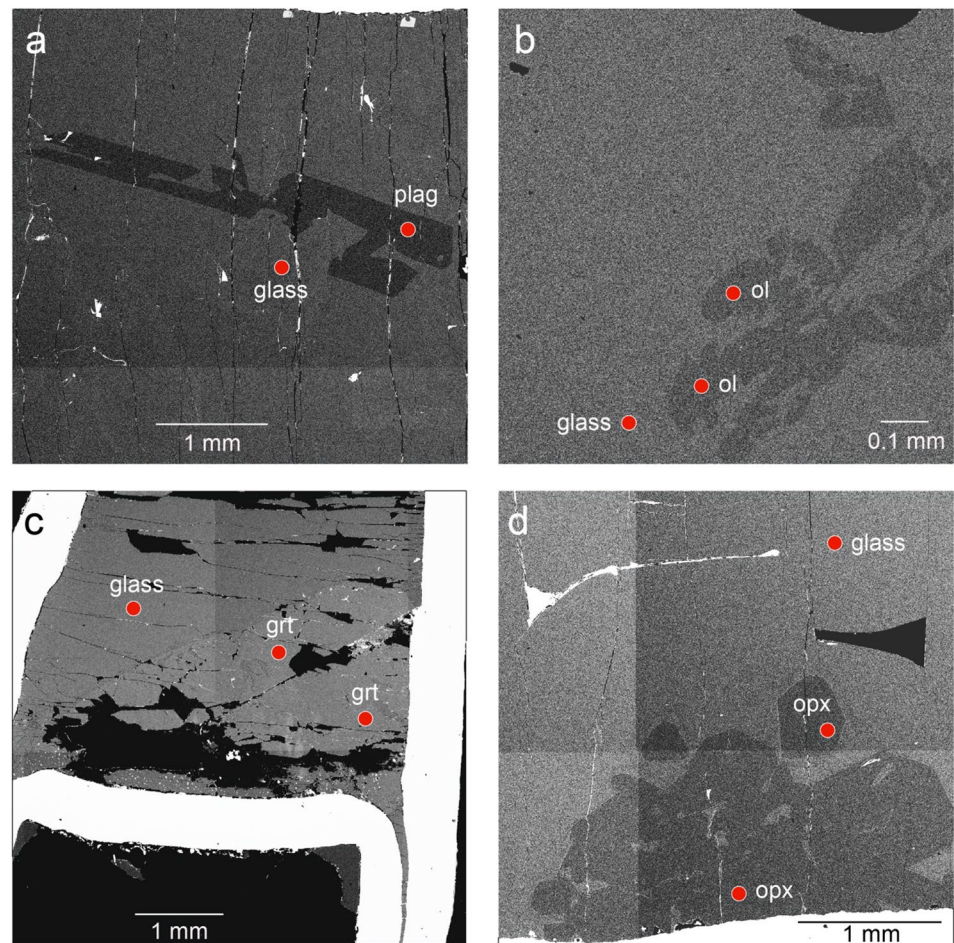
The degassing of midocean ridge basalts is currently the main mechanism transporting nitrogen from the mantle into the atmosphere. MORB melts are generated in the upper mantle where the ambient oxygen fugacity is within  $\pm 2$  log units of the QFM (quartz fayalite magnetite) buffer (Frost and McCammon 2008; for reference, the oxygen fugacity of Ni–NiO is just 0.5 to 1 log unit above QFM). More specifically, the oxygen fugacity recorded in natural MORBs is  $0.2 \pm 0.3$  log units above QFM (O'Neill et al. 2018). We will therefore calculate here the likely species distribution of nitrogen in MORB melts and associated fluids at pressures of 0.5 to 2 GPa, a temperature of 1300 °C and an oxygen fugacity at the QFM buffer.

Li and Keppler (2014) studied nitrogen speciation in aqueous fluids and parameterized.

$$K^* = \frac{x_{\text{NH}_3}^2}{x_{\text{N}_2}}, \quad (6)$$

where  $x$  are molar fractions, as a function of pressure ( $P$ ), temperature ( $T$ ) and redox conditions (relative to the log  $f\text{O}_2$  at Ni–NiO buffer conditions,  $\Delta\text{NNO}$ ):

**Fig. 9** Backscatter electron images of run products from partitioning experiments. The location of SIMS measurements is indicated by red spots. **a** run 3.18, **b** run 19.43, **c** run 21.45 (compare Fig. 8b), **d** run 8.24 (compare Fig. 8a). Figures **a**, **c**, and **d** are composites made from several images, the boundaries are visible as straight vertical or horizontal lines. *plag* plagioclase, *ol* olivine, *grt* garnet, *opx* orthopyroxene



$$\log K^* = -9.694 + 8272/T + 0.0211P - 0.8020\Delta\text{NNO}. \quad (7)$$

For the QFM buffer, 1300 °C and 0.5–2 GPa their regression Eq. (7) yields  $\log K^*$  ranging from  $-3.75$  to  $-3.78$ . For a molar fraction of nitrogen in the fluid of 0.1, this predicts a  $\text{NH}_3/\text{N}_2$  molar ratio in the fluid of 0.04. This is, however, in an aqueous fluid, i.e., at very high water fugacity. Under the rather low water fugacities prevailing in the MORB source mantle, according to Eq. (5), the  $\text{NH}_3/\text{N}_2$  ratio in a fluid should be much lower. The relevant water fugacities can be estimated from the water contents of primitive MORB magmas, which are typically in the range of 500–3000 ppm (e.g., Saal et al. 2002). Shishkina et al. (2010) studied water solubility in basalts as a function of water saturation pressure. They described their data by the equation  $c_{\text{water}} = 0.2351 P^{0.5758}$ , where  $c_{\text{water}}$  is the water solubility in the melt in wt.% and  $P$  is water pressure in MPa. For a water content of 0.3 wt.%, this yields a water saturation pressure of 1.52 MPa, which at these low pressures is essentially equal to water fugacity. If one assumes that in the experiments of Li and Keppler (2014) in an aqueous fluid phase, the water fugacity

was about the same as that of pure water at the given  $P$  and  $T$  conditions, Eq. (5) can now be used to predict the  $\text{NH}_3/\text{N}_2$  ratio in a fluid, assuming further that fugacities are proportional to molar fractions at otherwise equal conditions. For 1300 °C and QFM buffer conditions, this yields a corrected  $\log K^*$  ranging from  $-11.6$  for 0.5 GPa to  $-15.4$  at 2 GPa. For a  $\text{N}_2$  molar fraction in the fluid of 0.1, the calculated  $\text{NH}_3/\text{N}_2$  molar ratio then ranges from  $5 \cdot 10^{-6}$  to  $2 \cdot 10^{-7}$ . This calculation shows that the  $\text{NH}_3/\text{N}_2$  ratio expected in a fluid under conditions relevant for MORB is negligibly small. In a silicate melt, the ratio could in principle be different. This difference would manifest itself in a different partitioning of  $\text{N}_2$  and  $\text{NH}_3$  between a silicate melt and aqueous fluid. Indeed, Li et al. (2015) noted such a difference in their study of the fluid/melt partitioning of nitrogen. However, the difference between the nitrogen partition coefficient under oxidizing conditions, where  $\text{N}_2$  is predominant, and under reducing conditions, where  $\text{NH}_3$  prevails, is only about two orders of magnitude, such that even in a MORB melt, the fraction of nitrogen in reduced state should still be negligible. We therefore conclude that our data on  $\text{N}_2$  solubility and partitioning can be applied with confidence to model the behavior of nitrogen

**Table 3** Summary of experiments on the partitioning of nitrogen between minerals and basaltic melt

| Run no | Starting material | Silicate (mg) | Ag <sup>15</sup> N <sub>3</sub> (mg) | Pressure (GPa) | Temperature (°C) | Duration (hours) | Phases         | Nitrogen <sub>mineral</sub> (μg/g <sup>15</sup> N) | Nitrogen <sub>melt</sub> (μg/g <sup>15</sup> N) | D <sub>mineral/melt</sub>                          |
|--------|-------------------|---------------|--------------------------------------|----------------|------------------|------------------|----------------|--|---|--|
| 3.18   | MORB              | 126           | 4.5                                  | 2              | 1400–1250        | 4+24+72          | pl, cpx, melt  | 4.0 <sub>pl</sub> (9)<br>0.56 <sub>cpx</sub>       | 4258  | 0.0009 <sub>pl</sub> (2)<br>0.00013 <sub>cpx</sub> |
| 21.45  | Grt-MORB          | 167           | 1.7                                  | 4              | 1620–1500        | 7+30+48          | grt, melt      | 2.6 <sub>grt</sub>                                 | 2335  | 0.0011 <sub>grt</sub>                              |
| 19.43  | Opx-MORB          | 137           | 5.1                                  | 3              | 1500–unknown*    | 4+24+48          | ol, melt       | 0.53 <sub>ol</sub>                                 | 289   | 0.0018 <sub>ol</sub>                               |
| 8.24   | Ol-MORB           | 136           | 3.1                                  | 1.5            | 1400–1300        | 4+24+48          | opx, melt      | 0.98 <sub>opx</sub>                                | 742   | 0.0013 <sub>opx</sub>                              |
| 7.23*  | Ol-MORB           | 122           | 5.7                                  | 2.5            | 1400–unknown*    | 4+24+120         | opx, cpx, melt | 0.64 <sub>opx</sub><br>0.49 <sub>cpx</sub> (9)     | 428   | 0.0015 <sub>opx</sub><br>0.0011 <sub>cpx</sub> (2) |

All experiments were carried out in a piston cylinder apparatus by first heating above the liquidus, then cooling at a constant rate to a temperature between liquidus and solidus and then annealing at this temperature. The durations for these three steps are given in the sequence described. In the experiment marked with an asterisk (\*), the thermocouple failed during the run. Numbers in brackets are one standard deviation in the last digits; where no uncertainty is given, only one measurement was carried out. Starting materials were a glass of midocean ridge basalt (MORB) composition, or the same glass mixed with 15–30 wt.% of a mixture of MgO and SiO<sub>2</sub> of MgSiO<sub>3</sub> orthopyroxene composition (Opx-MORB) or of Mg<sub>2</sub>SiO<sub>4</sub> olivine composition (Ol-MORB). Grt-MORB is a mixture of the MORB glass with 30% of powder of a natural, almandine-rich garnet and a few large garnet seed crystals. Silicate and Ag<sup>15</sup>N<sub>3</sub> are the amounts of the silicate starting mixture and of Ag<sup>15</sup>N<sub>3</sub> initially loaded into the capsule

*cpx* clinopyroxene, *grt* garnet, *ol* olivine, *opx* orthopyroxene, *pl* plagioclase

during the degassing of the MORB mantle. Due to the much higher ambient oxygen fugacity, these parameters likely are also applicable to most melting and degassing processes in the crust. Only for particularly reduced and volatile-enriched mantle material, such as that sourced by some plume-related hotspots, or for the degassing of a perhaps more reduced mantle in the very early history of the Earth, they should not be directly applied.

## Geochemical applications

### N<sub>2</sub> as a possible trigger of vapor saturation in felsic magmas

Vapor saturation in magmas leads to the formation of gas bubbles (e.g., Shea 2017). The internal overpressure and expansion of such bubbles is the main driving force for rapid magma ascent and any kind of explosive volcanic activity. Moreover, the enrichment of trace elements in magmatic-hydrothermal systems (e.g., Audetat et al. 2008) critically depends on the timing of vapor saturation in relation to other events, such as sulfide precipitation. The conditions for vapor saturation in magmatic systems were so far nearly exclusively discussed in terms of saturation with a H<sub>2</sub>O–CO<sub>2</sub> gas phase (e.g., Duan, 2014). Here, we argue that for some felsic magmas, specifically those produced by re-melting of sedimentary precursor materials, it may well be that the N<sub>2</sub> content actually triggers vapor oversaturation. This is plausible, because the solubility of N<sub>2</sub> in silicic melts (Fig. 3) is very low, much lower than for CO<sub>2</sub>. Ni and Keppeler (2013) showed that the solubility of CO<sub>2</sub> in basaltic to rhyolitic melts may be described by an effective Henry constant of 0.567 ppm/bar or 5670 ppm/GPa. On a ppm by weight basis, this number is more than three times higher than that of N<sub>2</sub> in felsic melts and even on a molar basis, CO<sub>2</sub> solubility remains more than twice higher than N<sub>2</sub> solubility. Already a few hundred ppm of dissolved N<sub>2</sub> suffice for vapor saturation of a granitic melt in the shallow crust. Even in the middle crust, at a depth of 15 km, corresponding to about 0.5 GPa, less than 1000 ppm of N<sub>2</sub> are required for this effect. On the other hand, many sedimentary shales and metamorphic schists contain several hundred or even more than 1000 ppm of nitrogen (see the compilation in Johnson and Goldblatt 2015). It is, therefore, quite plausible that magmas that were produced by anatexic melting of such sources may contain sufficient N<sub>2</sub> such that this volatile will control the point of vapor saturation. This effect could be particularly important for typical “S-type granites” that are often associated with magmatic-hydrothermal Sn–W mineralization (Lehmann 2021).

**Table 4** Mineral and melt compositions from partitioning experiments

| Run no | Phase | SiO <sub>2</sub> | TiO <sub>2</sub> | Al <sub>2</sub> O <sub>3</sub> | MgO       | CaO      | FeO <sub>tot</sub> | Na <sub>2</sub> O | K <sub>2</sub> O | H <sub>2</sub> O | Total |
|--------|-------|------------------|------------------|--------------------------------|-----------|----------|--------------------|-------------------|------------------|------------------|-------|
| 3.18   | Glass | 53.4 (2)         | 2.19 (6)         | 16.7 (2)                       | 3.50 (1)  | 5.47 (9) | 8.12 (8)           | 3.8 (1)           | 0.47 (4)         | 0.29             | 93.9  |
|        | Plg   | 58.5 (4)         | 0.04 (1)         | 24.5 (2)                       | 0.07 (2)  | 7.22 (4) | 0.68 (2)           | 6.38 (1)          | 0.19 (1)         | –                | 97.5  |
|        | Cpx   | 47.2 (6)         | 0.89 (1)         | 12.6 (4)                       | 11.2 (5)  | 13 (1)   | 11.3 (2)           | 2.3 (1)           | –                | –                | 98.4  |
| 21.45  | Glass | 49.9 (3)         | 1.6 (1)          | 15.0 (2)                       | 4.41 (2)  | 7.7 (1)  | 12.5 (1)           | 2.4 (1)           | 0.20 (1)         | 1.71             | 95.4  |
|        | Grt   | 39.9 (4)         | 0.21 (4)         | 22.3 (5)                       | 13.4 (2)  | 6.4 (8)  | 16 (1)             | 0.06 (1)          | –                | –                | 98.7  |
| 19.43  | Glass | 58.1 (2)         | 1.0 (1)          | 12.5 (1)                       | 11.4 (1)  | 6.4 (1)  | 1.5 (1)            | 3.4 (1)           | 0.31 (1)         | 1.09             | 95.7  |
|        | Ol    | 41.5 (5)         | 0.05 (4)         | –                              | 55.1(3)   | 0.13 (1) | 2.6 (1)            | –                 | –                | –                | 99.4  |
| 8.24   | Glass | 47.4 (1)         | 1.47 (6)         | 13.7 (5)                       | 12 (1)    | 9.6 (2)  | 5.28 (1)           | 2.7 (7)           | 0.27 (3)         | 3.17             | 95.2  |
|        | Opx   | 57.6 (1)         | 0.11 (1)         | 1.7 (2)                        | 36.0 (1)  | 1.4 (1)  | 3.50 (2)           | 0.08 (1)          | –                | –                | 100.3 |
| 7.23   | Glass | 42.6 (3)         | 2.2 (1)          | 15.4 (1)                       | 10.9 (1)  | 8.5 (1)  | 6.0 (1)            | 2.8 (1)           | 0.34 (2)         | 0.10             | 88.7  |
|        | Cpx   | 51.8 (11)        | 0.40 (1)         | 8.0 (17)                       | 17.3 (17) | 16.3 (3) | 4.2 (4)            | 1.8 (3)           | –                | –                | 99.9  |
|        | Opx   | 54.0 (2)         | 0.15 (4)         | 5 (3)                          | 34 (2)    | 1.2 (2)  | 5 (1)              | 0.14 (6)          | –                | –                | 99.8  |

Compositions were measured by electron microprobe, except for H<sub>2</sub>O, which was measured by FTIR. Numbers in brackets are one standard deviation in the last digits.–indicates concentrations below detection limit. The low microprobe totals of the glasses are partially due to the fact that iron is reported as FeO only (FeO<sub>tot</sub>), while in reality, it is partially Fe<sub>2</sub>O<sub>3</sub>. Most of the effect, however, likely results from surface charging due to the high defect concentration in the glasses (Hughes et al. 2019). The glass in run 7.23 is difficult to measure due to numerous fine cracks produced upon decompression

*cpx* clinopyroxene, *grt* garnet, *ol* olivine, *opx* orthopyroxene, *pl* plagioclase

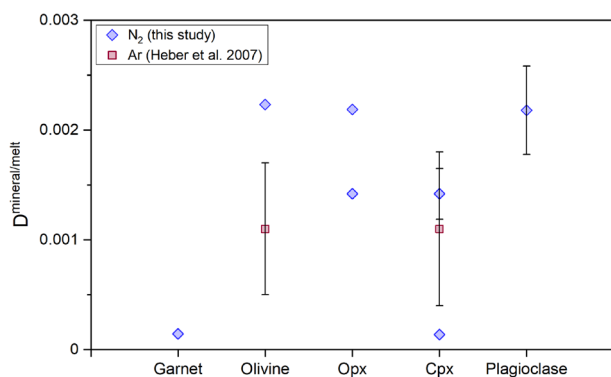


**Fig. 10** Comparison of the mineral/melt partition coefficients of nitrogen (this study) with the mineral/melt partition coefficients of argon (Heber et al. 2007). Where no error bars are shown, the uncertainties are not known, because only one measurement was performed

### Fractionation of nitrogen and argon during mantle melting

The question of whether or not nitrogen and argon are fractionated during mantle melting is of fundamental importance for constraining the Earth's deep nitrogen budget. Since nitrogen is highly volatile, it is likely, at least partially, to be lost from most mantle samples upon ascent to the surface and therefore, the initial mantle nitrogen content cannot be determined by the direct analysis of samples. Marty (1995) observed that the N<sub>2</sub>/<sup>40</sup>Ar ratio in MORB samples is nearly constant, despite large variations in the overall volatile content. This suggested that N<sub>2</sub> and Ar are not significantly fractionated during partial melting or degassing, such

that the measured N<sub>2</sub>/<sup>40</sup>Ar ratio may be representative for the mantle source. This observation allows one to estimate mantle nitrogen contents, since the abundance of <sup>40</sup>Ar, a radioactive decay product of <sup>40</sup>K, is well constrained (e.g., Marty 1995; Johnson and Goldblatt 2015). Current estimates of nitrogen abundances in the mantle, therefore, usually rely on N<sub>2</sub>/<sup>40</sup>Ar systematics (for an alternative approach, see Cartigny et al. 2001a). The data presented here for the first time allow a direct check of the validity of the underlying assumptions in such calculations. Contrary to what is conventionally assumed, there appears to be a fractionation between N<sub>2</sub> and Ar during mantle melting, with N<sub>2</sub> being more compatible, although the experimental data presented here have significant uncertainties (Fig. 9). However, the partition coefficients are so low that during plausible degrees of melting, e.g., during MORB generation (10–20% melting), nearly the entire budget of N<sub>2</sub> and Ar will enter the melt, such that both elements are indeed not fractionated. Only for very low-degree partial melts, some noticeable fractionation might occur. On the other hand, the solubility data in Fig. 7 clearly show that N<sub>2</sub> is less soluble in melts than Ar, which should cause some fractionation of Ar and N<sub>2</sub> during degassing. Indeed, Cartigny et al (2001b) investigated the relative contributions of source inhomogeneity and degassing to the variability of N<sub>2</sub>/Ar ratios in a large suite of MORB samples. With a two-stage degassing model (closed-system degassing followed by Rayleigh distillation), they were able to explain most of the variability. Their model suggests that Ar solubility in the MORB melt is about 1.2 times higher than N<sub>2</sub> solubility, in good agreement with our study. Overall, the data presented here therefore support the

reliability of estimated mantle nitrogen reservoirs based on  $N_2/^{40}Ar$  systematics, although some minor fractionations may occur both during melting and degassing.

**Acknowledgements** This study was supported by the DFG (Deutsche Forschungsgemeinschaft) International Research Training Group “Deep Earth Volatile Cycles”, DFG GRK 2156/1. Catherine McCammon kindly collected the Mossbauer spectra of the MORB glasses and Doro Wiesner took some BSE images of the samples. Constructive reviews by Stephen Parman and by an anonymous referee helped to improve the manuscript.

**Funding** Open Access funding enabled and organized by Projekt DEAL. Deutsche Forschungsgemeinschaft, GRK 2156/1, Hans Keppler.

**Open Access** This article is licensed under a Creative Commons Attribution 4.0 International License, which permits use, sharing, adaptation, distribution and reproduction in any medium or format, as long as you give appropriate credit to the original author(s) and the source, provide a link to the Creative Commons licence, and indicate if changes were made. The images or other third party material in this article are included in the article's Creative Commons licence, unless indicated otherwise in a credit line to the material. If material is not included in the article's Creative Commons licence and your intended use is not permitted by statutory regulation or exceeds the permitted use, you will need to obtain permission directly from the copyright holder. To view a copy of this licence, visit <http://creativecommons.org/licenses/by/4.0/>.

## References

- Audetat A, Pettke T, Heinrich CA, Bodnar RJ (2008) The composition of magmatic-hydrothermal fluids in barren and mineralized intrusions. *Econ Geol* 103:877–908
- Bernadou F, Gaillard F, Füre E, Marrocchi Y, Slodczyk A (2021) Nitrogen solubility in basaltic silicate melt - implications for degassing processes. *Chem Geology* 573:120192
- Borisov A, Behrens H, Holtz F (2018) Ferric/ferrous ratio in silicate melts: a new model for 1 atm data with special emphasis on the effects of melt composition. *Contrib Mineral Petrol* 173:98
- Bottinga Y (1985) On the isothermal compressibility of silicate liquids at high pressure. *Earth Planet Sci Lett* 74:350–360
- Boulliung J, Füre E, Dalou C, Tissandier L, Zimmermann L, Marrocchi Y (2020) Oxygen fugacity and melt composition controls on nitrogen solubility in silicate melts. *Geochim Cosmochim Acta* 284:120–133
- Brooker A, Holloway JR, Hervig R (1998) Reduction in piston-cylinder experiments: the detection of carbon infiltration into platinum capsules. *Am Mineral* 83:985–994
- Busigny V, Cartigny P, Philippot P, Ader M, Javoy M (2003) Massive recycling of nitrogen and other fluid-mobile elements (K, Rb, Cs, H) in a cold slab environment: evidence from HP to UHP oceanic metasediments of the Schistes Lustrés nappe (western Alps, Europe). *Earth Planet Sci Lett* 215:27–42
- Carroll MR, Stolper EM (1993) Noble gas solubilities in silicate and glasses: new experimental results for argon and the relationship between solubility and ionic porosity. *Geochim Cosmochim Acta* 57:5039–5051
- Carroll MR, Webster JD (1994) Solubilities of sulfur, noble gases, nitrogen, chlorine, and fluorine in magmas. *Rev Mineral* 30:231–279
- Cartigny P, Harris JW, Javoy M (2001a) Diamond genesis, mantle fractionations and mantle nitrogen content: a study of  $\delta^{13}C-N$  concentrations in diamonds. *Earth Planet Sci Lett* 185:85–98
- Cartigny P, Jendrzewski N, Pineau F, Petit E, Javoy M (2001b) Volatile (C, N, Ar) variability in MORB and the respective roles of mantle source heterogeneity and degassing: the case of the southwest Indian ridge. *Earth Planet Sci Lett* 194:241–257
- Duan X (2014) A general model for predicting the solubility behavior of  $H_2O-CO_2$  fluids in silicate melts over a wide range of pressure, temperature and compositions. *Geochim Cosmochim Acta* 125:582–609
- Frischat GH, Buschmann O, Meyer H (1978) Diffusion von Stickstoff in Glasschmelzen. *Glastech Ber* 51:321–327
- Frost DJ, McCammon CA (2008) The redox state of Earth's mantle. *Ann Rev Earth Planet Sci* 36:389–420
- Gale A, Dalton CA, Langmuir CH, Su Y, Schilling JG (2013) The mean composition of ocean ridge basalts. *Geochem, Geophys, Geosyst* 14:489–518
- Heber VS, Brooker RA, Kelley SP, Wood BJ (2007) Crystal-melt partitioning of noble gases (helium, neon, argon, krypton, and xenon) for olivine and clinopyroxene. *Geochim Cosmochim Acta* 71:1041–1061
- Holtz F, Behrens H, Dingwell DB, Johannes W (1995)  $H_2O$  solubility in haplogranitic melts - compositional, pressure, and temperature dependence. *Am Mineral* 80:94–108
- Hughes EC, Buse B, Kearns SL, Blundy JD, Kilgour G, Mader HM (2019) Low analytical totals in EPMA of hydrous silicate glass due to sub-surface charging: obtaining accurate volatiles by difference. *Chem Geol* 505:48–56
- Iacono-Marziano G, Paonita A, Rizzo A, Scaillet B, Gaillard F (2010) Noble gas solubilities in silicate melts: new experimental results and a comprehensive model of the effects of liquid composition, temperature and pressure. *Chem Geol* 279:145–157
- Johnson B, Goldblatt C (2015) The nitrogen budget of Earth. *Earth Sci Rev* 148:150–173
- Kadik AA, Kurovskaya NA, Ignat'ev YA, Kononkova NN, Koltashev VV, Plotnichenko VG (2011) Influence of oxygen fugacity on the solubility of nitrogen, carbon, and hydrogen in  $FeO-Na_2O-SiO_2-Al_2O_3$  melts in equilibrium with metallic iron at 1.5 GPa and 1400 °C. *Geochem Internat* 49:429–438
- Karl D, Letelier R, Tupas L, Dore J, Christian J, Hebel D (1997) The role of nitrogen fixation in biogeochemical cycling in the subtropical north Pacific ocean. *Nature* 388:533–538
- Keppler H (1989) A new method for the generation of  $N_2$ -containing fluids in high-pressure experiments. *Eur J Mineral* 1:135–137
- Kesson SE, Holloway JR (1974) The generation of  $N_2-CO_2-H_2O$  fluids for use in hydrothermal experimentation. II. Melting of albite in a multispecies fluid. *Am Mineral* 59:598–603
- Labidi J, Barry PH, Bekaert DV, Broadley MV, Marty B, Giunta T, Warr O, Sherwood Lollar B, Fischer TP, Avice G, Caracausi A, Ballentine CJ, Halldórsson SA, Stefánsson A, Kurz MD, Kohl IE, Young ED (2020) Hydrothermal  $^{15}N/^{14}N$  abundances constrain the origins of mantle nitrogen. *Nature* 580:367–371
- Lehmann B (2021) Formation of tin ore deposits: a reassessment. *Lithos* 402–403:105756
- Li Y, Keppler H (2014) Nitrogen speciation in mantle and crustal fluids. *Geochim Cosmochim Acta* 129:13–32
- Li Y, Huang R, Wiedenbeck M, Keppler H (2015) Nitrogen distribution between aqueous fluids and silicate melts. *Earth Planet Sci Lett* 411:218–228
- Li Y, Wiedenbeck M, Shcheka S, Keppler H (2013) Nitrogen solubility in upper mantle minerals. *Earth Planet Sci Lett* 377:311–323
- Libourel G, Marty B, Humbert F (2003) Nitrogen solubility in basaltic melt. part I. effect of oxygen fugacity. *Geochim Cosmochim Acta* 67:4123–4135

- Mallik A, Li Y, Wiedenbeck M (2018) Nitrogen evolution within the earth's atmosphere–mantle system assessed by recycling in subduction zones. *Earth Planet Sci Lett* 482:556–566
- Marty B (1995) Nitrogen content of the mantle inferred from N<sub>2</sub>-Ar correlation in oceanic basalts. *Nature* 377:326–329
- Marty B, Yokochi R (2006) Water in the early Earth. *Rev Mineral Geochem* 62:421–450
- Miyazaki A, Hiyagon H, Sugiura N, Hirose K, Takahashi E (2004) Solubilities of nitrogen and noble gases in silicate melts under various oxygen fugacities: implications for the origin and degassing history of nitrogen and noble gases in the earth. *Geochim Cosmochim Acta* 68:387–401
- Mysen BO, Yamashita S, Chertkova N (2008) Solubility and solution mechanisms of NOH volatiles in silicate melts at high pressure and temperature - amine groups and hydrogen fugacity. *Am Mineral* 93:1760–1770
- Ni H, Keppler H (2013) Carbon in silicate melts. *Rev Mineral Geochem* 75:251–287
- O'Neil, HughBerry St CAJ, Mallmann G (2018) The oxidation state of iron in Mid-Ocean Ridge Basaltic (MORB) glasses: Implications for their petrogenesis and oxygen fugacities. *Earth Planet Sci Lett* 504:152–162
- Roskosz M, Mysen BO, Cody GD (2006) Dual speciation of nitrogen in silicate melts at high pressure and temperature: an experimental study. *Geochim Cosmochim Acta* 70:2902–2918
- Saal AE, Hauri EH, Langmuir CH, Perfit MR (2002) Vapour undersaturation in primitive mid-ocean-ridge basalt and the volatile content of Earth's upper mantle. *Nature* 419:451–455
- Sano Y, Takahata N, Nishio Y, Fischer TP, Williams SN (2001) Volcanic flux of nitrogen from the Earth. *Chem Geol* 171:263–271
- Schmidt BC, Holtz FM, Bény JM (1998) Incorporation of H<sub>2</sub> in vitreous silica, qualitative and quantitative determination from Raman and infrared spectroscopy. *J Non-Crystalline Solids* 240:91–103
- Shea T (2017) Bubble nucleation in magmas: a dominantly heterogeneous process? *J Volcanol Geothermal Res* 343:155–170
- Schmidt BC, Keppler H (2002) Experimental evidence for high noble gas solubilities in silicate melts under mantle pressures. *Earth Planet Sci Lett* 195:277–290
- Shishkina TA, Botcharnikov RE, Holtz F, Almeev RR, Portnyagin MV (2010) Solubility of H<sub>2</sub>O- and CO<sub>2</sub>-bearing fluids in tholeiitic basalts at pressures up to 500 MPa. *Chem Geol* 277:115–125
- Wang Y, Sakamaki T, Skinner LB, Jing Z, Yu T, Kono Y, Park C, Shen G, Rivers ML, Sutton SR (2014) Atomistic insight into viscosity and density of silicate melts under pressure. *Nature Comm* 5:3241
- White BS, Brearley M, Montana A (1989) Solubility of argon in silicate liquids at high-pressures. *Am Mineral* 74:513–529
- Yoshioka T, McCammon C, Shcheka S, Keppler H (2015) The speciation of carbon monoxide in silicate melts and glasses. *Am Mineral* 100:1641–1644
- Yoshioka T, Wiedenbeck M, Shcheka S, Keppler H (2018) Nitrogen solubility in the deep mantle and the origin of Earth's primordial nitrogen budget. *Earth Planet Sci Lett* 488:134–143

**Publisher's Note** Springer Nature remains neutral with regard to jurisdictional claims in published maps and institutional affiliations.